Article

Micro- and Nano-Pollutants from Tires and Car Brakes Generated in the Winter Season in the Poznan City Urban Environment

Robert E. Przekop [1],[*] [ID], Bogna Sztorch [1], Daria Pakuła [1], Eliza Romańczuk-Ruszuk [2] [ID], Roksana Konieczna [1] and Miłosz Frydrych [1],[*] [ID]

[1] Centre for Advanced Technologies, Adam Mickiewicz University Poznan, Uniwersytetu Poznańskiego 10, 61-614 Poznań, Poland; bogna.sztorch@amu.edu.pl (B.S.); daria.pakula@amu.edu.pl (D.P.); roksana.konieczna@amu.edu.pl (R.K.)

[2] Institute of Biomedical Engineering, Faculty of Mechanical Engineering, Bialystok University of Technology, Wiejska 45C, 15-351 Bialystok, Poland; e.romanczuk@pb.edu.pl

[*] Correspondence: r.przekop@gmail.com or rprzekop@amu.edu.pl (R.E.P.); frydrych@amu.edu.pl (M.F.)

Abstract: This research, focusing on the environmental impact of tire and brake disc pad wear, constitutes a significant area of transport-related studies. These two key vehicle components are not only the most frequently worn but also generate micro- and nano-pollutants (i.e., rubber, metal oxides) that potentially harm the environment. Over half of the globally produced natural and synthetic rubbers, which amounted to about 30 million tons in 2022, are used for tire production. This work focuses on the study of roadside snow, sand, and standing water deposits from various locations in the urban agglomeration (Poznań, Poland) during the winter season, determining their qualitative composition and the quantitative content of pollutants originating from tire abrasion. In addition, the method of washing nano- and micro-rubber particles and their full characteristics was also presented. Fourier-transform infrared (FT-IR) and nuclear magnetic resonance (NMR) spectroscopic studies, optical and scanning electron microscopy (SEM-EDS), particle size studies using a dynamic light scattering (DLS) particle analyzer, and thermogravimetric analysis (TGA) were conducted for a detailed characterization of the pollutants in the environment. The conducted particle separation methods allowed for the extraction of a fraction mainly containing gum residues with particle sizes less than 2 μm. The results of these tests make it possible to estimate the level of contamination with rubber and metal residues during the abrasion of tires, pads, and brake discs while driving, which is crucial for understanding the impact of vehicle part exploitation on the environment.

Keywords: tire; rubber; metal oxides; environmental pollution; nanoparticles; microparticles

1. Introduction

Tire abrasion occurs during the power transfer where the tire makes contact with the road, engaging with diverse elements such as leftover leaves, soil fragments, sand, and water. Consequently, the abrasion is not solely attributed to tire degradation but rather to a combination of various substances. In the literature, the term "tire road and wear particle" (TRWP) is often used, even when referring to a mixture of particles originating from tire wear and road surfaces. In addition to larger particles that settle on the road or are transported to roadside soils or surface waters, there is also a fraction of smaller particles that can be carried by the air. This fraction plays a significant role in public health hazards and accounts for a maximum of 10% of the total mass emission associated with tire wear [1]. Non-exhaust particle emissions arise from abrasion of the brakes and tires and wear of the road surface, as well as from resuspension of road dust. These particles exhibit a diverse morphology, manifesting in various shapes. They are characterized by significant porosity, which contributes to their unique physical properties [2]. Furthermore, their qualitative

composition may differ from the original material, indicating a chemical transformation during the formation process [3].

The tire manufacturing industry utilizes approximately 60% of produced natural and synthetic rubbers. Tires have varying compositions depending on their intended application but most commonly consist of natural rubber, styrene-butadiene, and butadiene. During wear, they undergo abrasion, leading to the formation of so-called Tire Wear Particles, which contaminate the environment along with concurrently abraded road materials (i.e., bitumen, aggregate) [4]. In the research conducted by Stalnaker et al., it was demonstrated that the degree of tire wear, which is associated with the release of a larger amount of pollutants, is several times higher in urban agglomerations than during highway driving [5]. This is related to more dynamic driving, frequent braking, and maneuvering. This phenomenon can be attributed to the complex driving conditions in urban areas, characterized by frequent starts and stops, as well as the need for constant maneuvering due to traffic congestion. These factors contribute to accelerated tire wear and, subsequently, an increased release of pollutants [6].

The emissions of these particles can be categorized as non-airborne, which constitute over 90% of total emissions, and airborne [7]. It is assumed that the primary source of metals released into the environment are particles resulting from tire friction and brake disc and pad wear [8], such as iron, lead, chromium, copper, titanium, and many others [9–13]. Additionally, it is estimated that as a result of the abrasion of these materials, up to 1,327,000 tons of tire wear particles are produced annually within the European Union alone [8]. Reports are available presenting various tire brands with the amount of worn material during driving. In 2021, ADAC (Allgemeiner Deutscher Automobil-Club) presented a report in which the mass of particles generated as a result of winter tire abrasion while driving was determined for selected tire models, these data are presented in Table 1 [14].

Table 1. Data based on the ADAC report of December 2021, München [14].

Trade Name of the Type of Winter Tire Tested	Mass of Tires Wearing Out While Driving [g/1000 km]	Trade Name of the Type of Winter Tire Tested	Mass of Tires Wearing Out While Driving [g/1000 km]
BF Goodrich G-Force Winter 2	100	Barum Polaris 5	143
Michelin Alpin 6	105	Continental Winter Contact TS860	145
Vredestein Wintrac	109	GT Radial Winter Pro 2	149
General Tire Altimax Winter 3	124	Laufenn i Fit+ LW31	159
Nokian WR Snowproof	127	Yokohama Bluearth*Winter V906	163
Dunlop Winter Response-2	132	Falken Eurowinter HS01	164
Goodyear Ultra Grip 9+	134	Maxxis Premitra Snow WP6	167
Kumho Wintercraft WP51	137	Bridgestone Blizzak LM005	171

These particles are one of the main sources of microplastic pollution in both aquatic and terrestrial environments [6,15–17]. It is important to note that the majority of pollutant emissions come from tires rather than brakes. In combustion engine vehicles, over 45% of emissions stem from tire wear, while only 25% are derived from brakes. Furthermore, conducted studies have revealed that due to the increased weight of electric motor vehicles, this emission escalates to 61%. This highlights the significant role of tire wear in vehicular pollution, a factor that warrants further investigation, particularly in the context of the growing prevalence of electric vehicles [18–20].

In the scientific literature, there are known examples of studies aimed at detecting and quantifying particulate matter resulting from tire and road wear. These particles have been identified in various environments, including soil, road tunnels, snow deposits, and

aquatic ecosystems [8,15,21–25]. Simulative studies were also conducted under laboratory conditions to determine the content of tire wear particles. It was observed that the emission of particles varies depending on changes in driving conditions. Physicochemical analyses of these pollutants revealed a high content of carbon and silicon, heavy metals, sulfur, and mineral substances [26–28]. Research conducted by Tonegawa and Sasaki demonstrated that under such conditions, the release coefficient of airborne particles (PM_{10}, $PM_{2.5}$) is merely about 4% of the mass. Consequently, the majority of pollutants from tire residues remain on road surfaces [28,29]. The methodologies presented in these studies are comprehensive, encompassing sample preparation procedures for subsequent analysis. However, these studies underscore the absence of standardized methods, which impedes the uniformity of the results presented across different research efforts. Furthermore, scientists Mennekes and Nowack in their article highlight the fact that a significant majority of studies are based on the collection of already available data and the estimation of Tire Wear Particle quantities, rather than on an actual determination and conducting of an investigation [30].

There are many studies on the impact of these particles on the aquatic environment [31–37]. Research on the toxicity of these pollutants indicates that they have a detrimental effect on the photosynthesis of aquatic plants and exert toxic effects on certain filter-feeding species, such as Daphnia magna [15,38]. Given the potential environmental impact of these particles, it is crucial to determine local emissions in various environments. This will allow for more extensive data collection and enable a more accurate estimation of the pollution level in different regions.

Further research is needed to develop standardized methods for the detection and quantification of these particles. This will not only improve the consistency of the results across different studies but also contribute to a better understanding of the environmental impact of tire and road wear particles. Moreover, the development of mitigation strategies to reduce the emission of these particles and their subsequent environmental impact should be a priority for future research [4,6,39].

This study explores the characteristics of micro- and nano-pollutants collected from snow deposits, roadside sand, and standing water samples from various locations within an urban agglomeration (Poznań, Poland). Subsequently, fractions primarily composed of tire particles were isolated from the obtained sediments using a washing method involving organic solvents such as isopropanol and dichloromethane. Subsequently, to identify and characterize the obtained materials, spectroscopic studies (X-ray Diffraction (XRD), Fourier-Transform Infrared Spectroscopy (FT-IR), and Nuclear Magnetic Resonance (NMR)), particle size measurement (Dynamic Light Scattering (DLS)), optical and scanning electron microscopy (SEM-EDS), and thermogravimetric analysis (TGA) were conducted.

2. Materials and Methods

2.1. Materials

The chemicals were purchased from the following sources: dichloromethane (DCM) and isopropanol (iPrOH) from Chempur, Piekary Slaskie, Poland; chloroform-d from Deutero, Gdansk, Poland. The filtering process was carried out on filter paper with a 5–13 μm pore size.

2.2. Preparation of Samples for Testing

Samples for analysis were collected during the winter from various points located in Poznań, Poland, as indicated on the map (Figure 1, Table 2). The samples were in the form of snow, precipitation water, or sand. This city is situated in the western region of Poland, on the Greater Poland Lake District, along the Warta River, and has a population of over 540,000 (as of 2023).
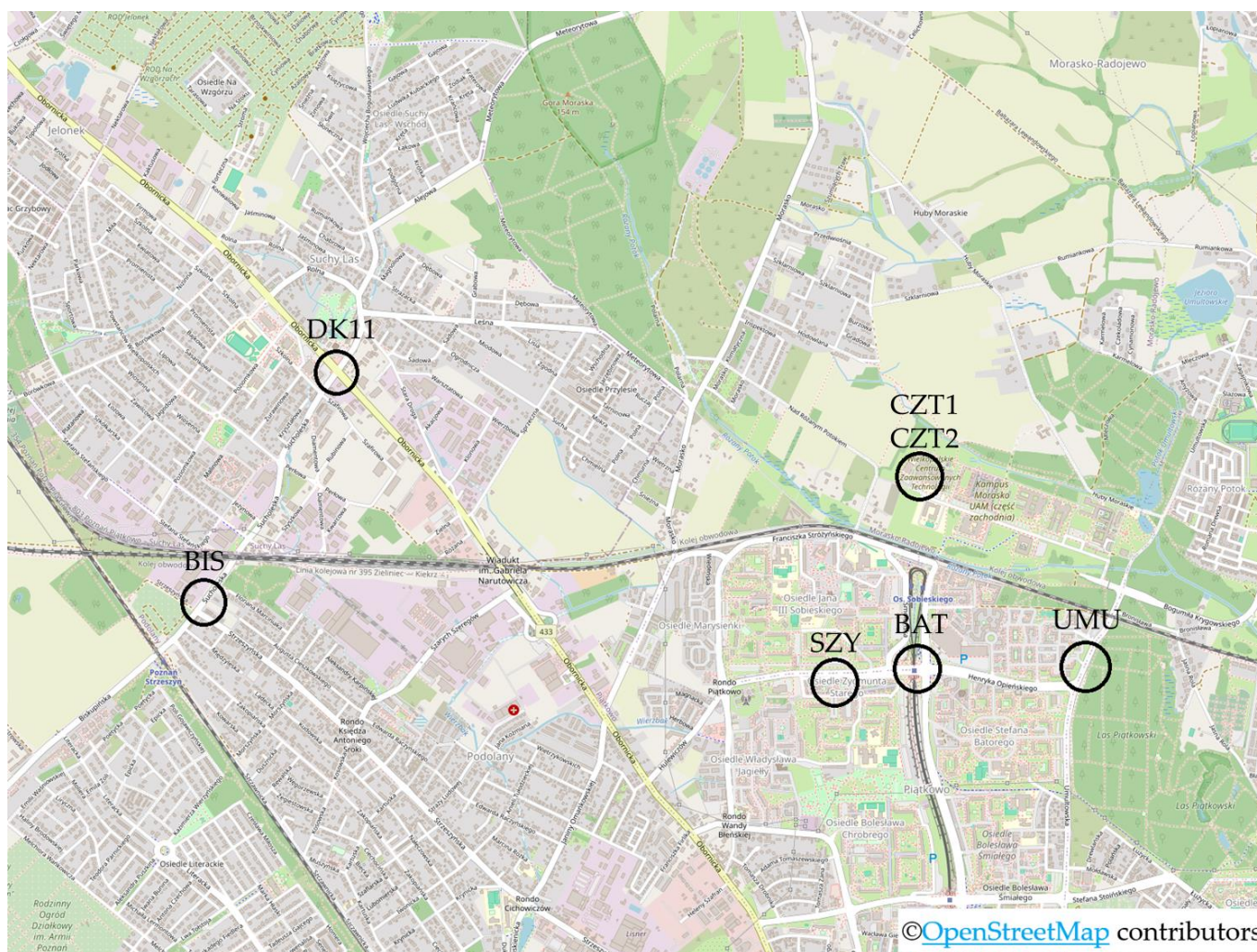
Figure 1. Map with marked locations where samples were collected for research (map data from ©
OpenStreetMap).

Table 2. List of collected samples along with their abbreviations and type.

No.	Place of Sample Collection	Abbreviation	Sample Type
1	Szymanowskiego street	SZY	Roadside sand
2	Umultowska street	UMU	Roadside sand
3	Biskupińska street	BIS	Roadside sand
4	Parking on the Morasko campus	CZT1	Snow deposit
5	Parking on the Morasko campus	CZT2	Snow deposit
6	Parking lot at the Stefan Batory estate	BAT	Standing water
7	DK11 street	DK11	Snow deposit

Snow, along with contaminants, was dissolved on a filter (and the remaining sediment
was rinsed with iPrOH (extract 1); then, the same sediment was washed with DCM (extract
2). The obtained fractions were concentrated in order to determine the concentrations of
dissolved particles, and then solutions of equal concentrations were prepared from them
(Figure 2).

For each extract, spectroscopic characterization (FT-IR and NMR) and microscopic analysis (SEM-EDS) were conducted, particle sizes were determined (DLS), and thermogravimetric analysis (TGA) was performed under nitrogen and air atmospheres.

Figure 2. Photo of standard solutions of particle fractions made in isopropanol and dichloromethane.

The residue remaining after extraction was sieved using a vibratory sieve, separating fractions >1 mm, 250 μm–1 mm, 100–250 μm, 40–100 μm, 25–40 μm, and <25 μm, which were then characterized using spectroscopic methods (FT-IR), microscopic techniques (optical, SEM-EDS), and thermogravimetric analysis (TGA). Particle size measurement was conducted for selected fractions, namely 40–100 μm, 25–40 μm, and <25 μm (DLS).

2.3. Determining the Concentrations of Tire Wear Particles

Samples of snow and street sediments, collected from various locations, underwent a multi-step extraction process using isopropanol and dichloromethane. This multi-stage procedure aimed to effectively remove contaminants and concentrate the particles present in the samples (Table 3). Subsequently, the solvents were evaporated using a laboratory evaporator, and the particle content was determined. Depending on the sampling location, such as roadside or parking areas, the concentration of extracted particles varied. The multi-step washing process and subsequent particle content analysis allowed for the determination of the chemical composition and morphology of particles from different locations.

Table 3. Comprehensive table of micro- and nano-pollutant concentrations in the sediments, recalculated to the dry mass of the sample (excluding water).

Sample	Solvent	Concentration [mg/100 g]
SZY	DCM [a]	6.95
	iPrOH [b]	16.27
UMU	DCM	11.54
	iPrOH	16.39
BAT	DCM	37.84
	iPrOH	48.65
CZT1	DCM	18.67
	iPrOH	52.01
BIS	DCM	5.82
	iPrOH	8.71
DK11	DCM	1.58
	iPrOH	11.92
CZT2	DCM	22.78
	iPrOH	23.23

[a] dichloromethane. [b] isopropanol.

2.4. Methods

Thermogravimetry (TGA) was performed using a NETZSCH 209 F1 Libra gravimetric analyzer (Selb, Germany). Samples of 5 ± 0.2 mg were placed in Al_2O_3 crucibles. Measurements were conducted under nitrogen and air (flow of 20 mL/min) in the range of 30–800 °C and 10 °C/min heating rate.

^{1}H and ^{29}Si nuclear magnetic resonance (NMR) spectra were recorded at 25 °C on Bruker Ascend 400 and Ultra Shield 300 (Billerica, MA, USA) spectrometers using $CDCl_3$ as a solvent. Chemical shifts are reported in ppm regarding the residual solvent ($CHCl_3$) peak for ^{1}H and ^{13}C.

Fourier-transform infrared (FT-IR) spectra were recorded on a Nicolet iS50 Fourier-transform spectrophotometer (Thermo Fisher Scientific, Waltham, MA, USA) equipped with a diamond ATR unit with a resolution of 0.09 cm^{-1}.

Particle size distribution of pollution particles was determined by a Mastersizer 3000 (Malvern Instruments Co. Ltd., Malvern, UK) using the laser diffraction method for powder substances using the Aero-S dry dispersion system and, for liquids, Hydro-UV wet dispersion. The analyses were conducted in isopropyl alcohol at room temperature. Five independent measurements in three series were taken for each sample.

A digital light microscope Keyence VHX 7000 (Keyence International, Mechelen, Belgium) with 100–×1000 VH-Z100T lens was used to examine the obtained material. All images were recorded with a VHX 7020 camera.

Sample surface morphology and chemical composition (SEM-EDS) were analyzed using a Phenom XL (Thermo Fisher Scientific) scanning electron microscope with resolution <20 nm.

X-ray diffraction studies were carried out on a Bruker D8 Eco Advance X-ray (Mannheim, Germany) diffractometer to determine the phase structure of the samples. The diffractometer works in geometry θ–2θ with a Cu-Kα lamp (λ = 0.15406 nm). The following parameters were used for measurements: radiation 40 kV and 25 mA, angular range 2θ 15–70°, step width 0.01°, and step time 3 s.

3. Results and Discussion

3.1. Microscopic Analysis

3.1.1. Optical Microscopic Analysis

To preliminarily ascertain the composition of individual fractions post-extraction, microscopic images of the acquired sediments were captured using an optical microscope (Figure 3). The analysis revealed that sand was predominant in all fractions. Fractions containing particles within the range >40 μm (Figure 3C–E) exhibited the presence of organic matter (such as plant fragments, etc.). Additionally, dark artifacts observed in the microscopic images were identified as iron particles.

This hypothesis was experimentally validated through SEM-EDS. Leveraging the magnetic properties of iron, its particles were isolated from the systems using a magnet. The presence of iron in the samples is most likely associated with the abrasion of brake pads during their usage (Figure 4).
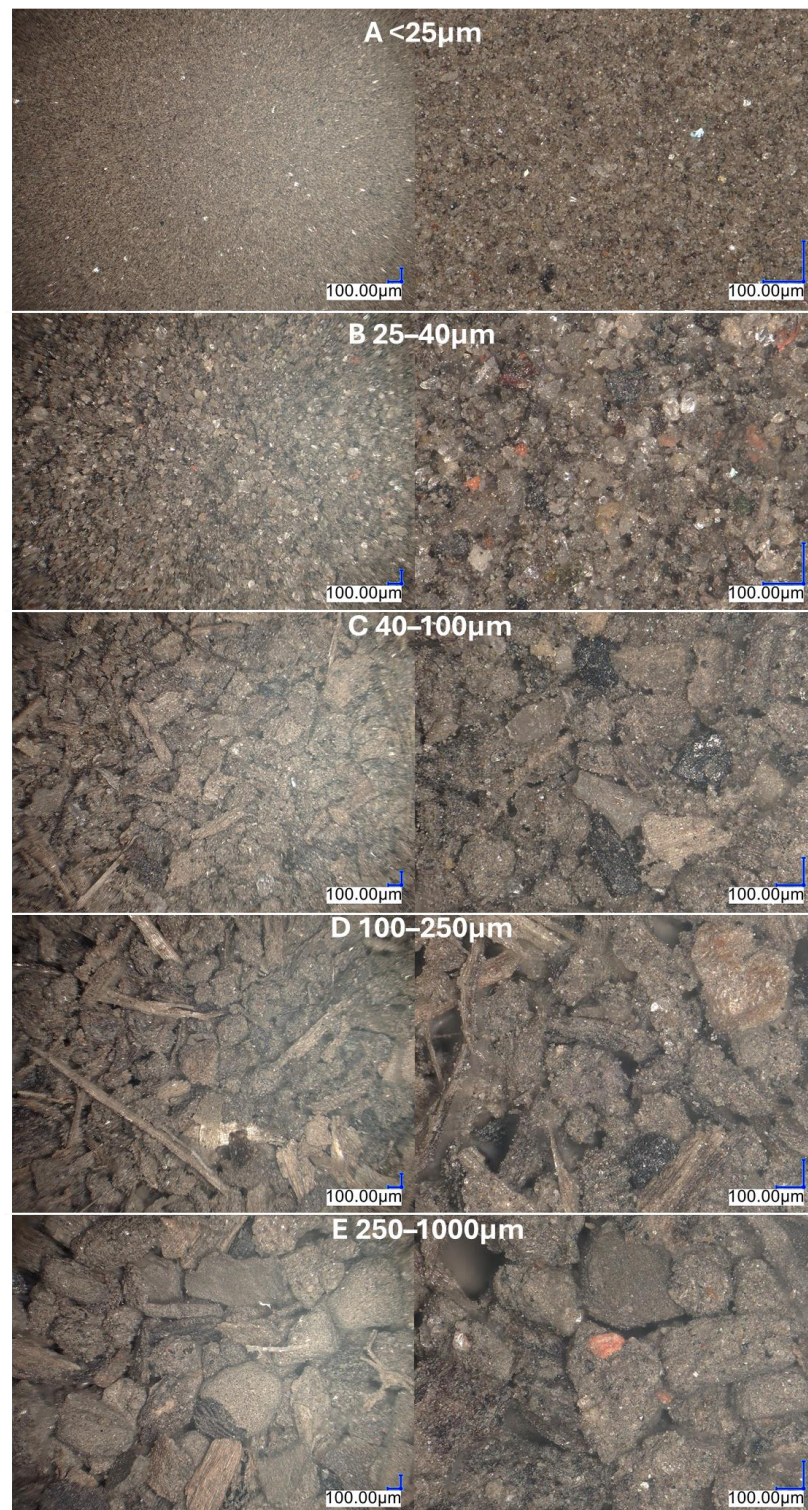
Figure 3. Microscopic images of all isolated sediment fractions obtained from BIS DCM.

Figure 4. Microscopic images of sediment samples of fractions below 25 μm and particles separated using a magnet.

3.1.2. SEM-EDS Analysis

Figures 5 and 6 illustrate the morphology of the fractionated sediment samples and products of extraction with organic solvents. The samples under consideration display irregular geometry and shape, with their dimensions correlating with the implemented fractionation procedure. The powders within a fraction of less than 25 μm exhibit a flake-like morphology, while particles exceeding 25 μm demonstrate angular characteristics. Particles of smaller size also present an acicular morphology. It is noteworthy that the particles within the fraction of less than 25 μm encompass a range of sizes, including very small particles (less than 10 μm) and larger particles (greater than 10 μm). In contrast, larger fractions are characterized by particles of more uniform sizes and consistent shapes. Predominantly, these particles display a combination of rounded and angular shapes. Additionally, EDS was performed, and the results are compiled in Table 4. Depending on the samples' origin, they display diverse chemical compositions.

Table 4. Elemental composition of selected materials obtained by EDS analysis.

Sample Name	Element Symbol | Atomic Concentration [%]														
BAT sediment	O	57.05	Ca	12.49	C	21.09	N	9.37							
BAT sediment	O	59.77	Si	10.00	Al	10.04	Na	8.51	C	11.35					
SZY sediment	O	57.17	Si	14.06	C	17.41	Al	5.47	Na	5.69	Te	0.16			
SZY sediment	O	57.36	C	29.75	Ca	8.21	Na	1.85	Cl	1.04	Si	1.19	Al	0.51	
BIS sediment	O	65.97	Si	12.39	Fe	5.12	Al	9.88	Mg	4.20	K	1.77			
CZT2 sediment	O	65.84	Si	12.69	Al	8.84	C	12.63							
UMU sediment	O	60.98	Si	9.67	Al	8.95	Fe	3.13	C	13.86	Na	1.39	Te	0.24	Cl	0.52
DCM extracts *	C	100													

* In EDS observations it was noticed that all samples of DCM extracts contained only carbon.
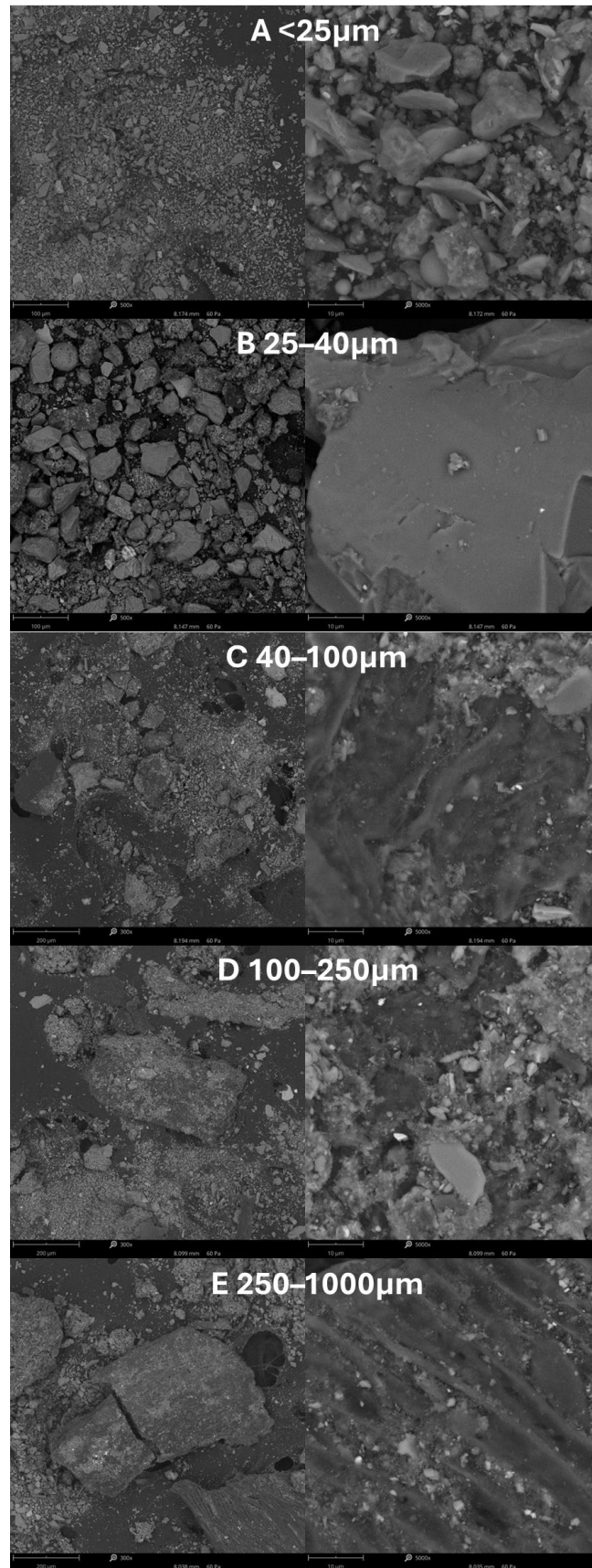
Figure 5. SEM images of all isolated sediment fractions obtained from BIS DCM.
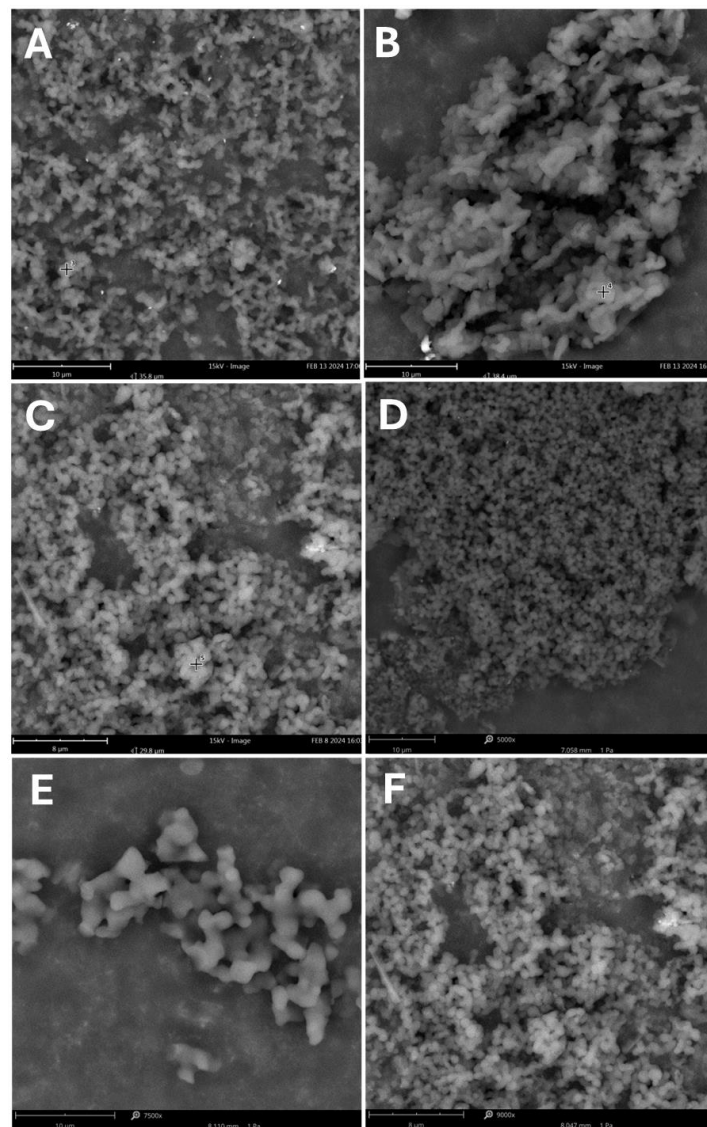
Figure 6. SEM images taken for extracts after washing with organic solvents: (**A**) UMU, (**B**) BIS, (**C**) BAT, (**D**) SZY, (**E**) CZT1, (**F**) DK11.

Samples collected from roadside sand contained a higher concentration of mineral components, such as calcium, aluminum, sodium, and metals like iron, likely originating from the wear and tear of brake pads. Furthermore, tellurium was detected in these samples. The sources and confirmation of its presence in the surface layer of soil at the sampling site have been extensively described in the work by Filella et al. [40].

EDS analysis of materials obtained from melted snow did not reveal the presence of calcium, which is consistent with the information provided in the section discussing thermogravimetric analysis (Section 3.3).

SEM images of organic-solvent-extracted and concentrated rubber particles are depicted in Figure 6. These particles exhibit a spherical shape and tend to agglomerate, leading to the formation of larger clusters with sizes smaller than 2 μm. The precise sizes of these particles were further examined using the DLS technique, which is described below.

The EDS analysis of all samples (Figure 6A–F) revealed only the presence of carbon. This further confirms that the organic fractions extracted contain rubber particles originating from car tires.

3.2. Determination of Particle Distribution

For post-extraction samples containing significant amounts of dry sediment, DLS particle size studies were conducted (Table 5). The homogeneity of the distribution, the surface area of the particles, and the Dx (10, 50, 90) values were established (Dx represents the appropriate threshold value, where 10%, 50%, and 90% of particles are less than or equal to this value). These studies, like sieve size measurements from optical microscopy and SEM, confirmed the effective separation of the material into individual fractions. Depending on the source of the samples, there are differences in their specific surface area and homogeneity; for example, the CZT2 sample from snow deposits is characterized by less homogeneity and also the largest specific surface area of the 25–40 μm fraction.

Table 5. Sediment particle size distribution based on DLS.

Sample	Fraction	Homogenity	Surface Area [m²/kg]	Dx (10) [μm]	Dx (50) [μm]	Dx (90) [μm]
SZY	<25 μm	0.901	1329	1.93	7.73	24.0
	25–40 μm	0.765	553.2	4.01	42.3	109
	40–100 μm	0.925	511.7	4.15	58.2	165
CZT2	<25 μm	0.871	1409	1.91	6.93	20.4
	25–40 μm	1.569	909.4	2.60	15.54	83.5
	40–100 μm	3.007	144.1	62.4	229	2230
UMU	<25 μm	0.733	1031	2.54	10.8	27.9
	25–40 μm	0.567	321.6	10.6	48.4	105
	40–100 μm	0.957	489.8	3.77	59	168
BIS	<25 μm	0.676	998	2.68	10.9	26.4
	25–40 μm	0.702	367.8	8.4	46.3	113
	40–100 μm	0.554	182.6	22.6	120	251

The particle size distribution obtained by extraction with isopropanol and dichloromethane is presented in Figure 7. The size of the majority of samples falls within the range of 0.01–0.5 μm for the isopropanol fraction and 0.01–0.3 μm for the dichloromethane fraction. Depending on the source of the material, particles of varying sizes are washed out. The extraction of sands with isopropanol (SZY, UMU, BIS) resulted in the acquisition of particles with sizes predominantly between 0.04 and 0.05 μm. However, when the starting material was snow, the sizes were CZT2 0.055 μm, CZT1 1.0 μm, and DK11 0.1 μm, respectively. Subsequent washing with dichloromethane leads to the extraction of smaller particles, with their sizes being more similar to each other.
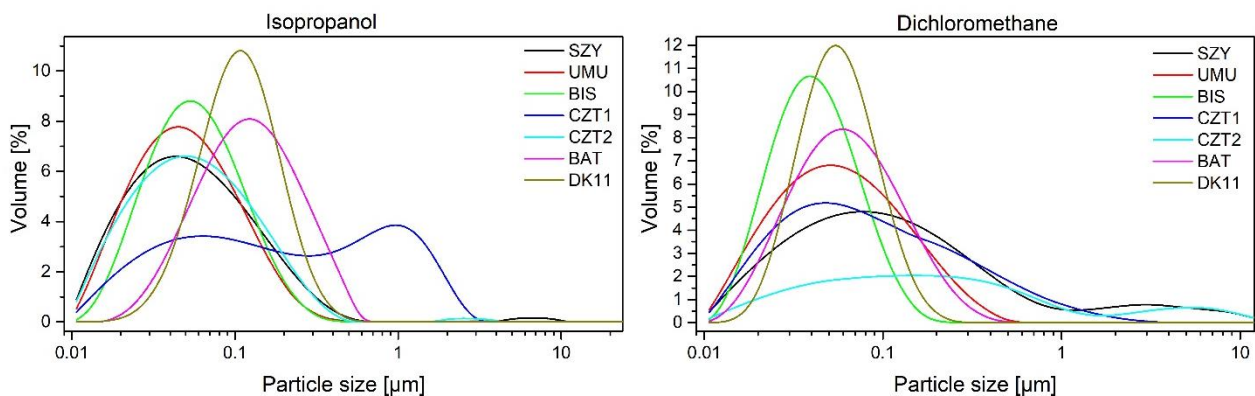

Figure 7. Particle size distribution in solutions after extraction with isopropanol and dichloromethane.

3.3. Thermogravimetric Analysis (TGA)

TGA of the dry extracts (DCM, iPr) was performed to analyze the content of the components of the nano rubber particles. Furthermore, experiments were performed for selected sediments with fractions <25 μm, 25–40 μm, 40–100 μm, 100–250 μm, and 250 μm–1 mm to ascertain the presence of organic and other compounds, which were washed with both dichloromethane and isopropanol. The analysis was conducted under inert gas and air atmospheres. From the TGA data, the residue mass and temperatures corresponding to the maximum decomposition rates (T_{max}) were determined.

In Figure 8, thermograms of dry extracts for analysis conducted in the nitrogen atmosphere (Figure 8A) and air atmosphere (Figure 8B) are presented. In the nitrogen atmosphere, a one-step decomposition of the dichloromethane extract is observed with a T_{max} = 445.8 °C, corresponding to the thermal degradation of polymers (nano rubber). Thermal analysis results indicate that washing with dichloromethane effectively enabled the extraction of nanoparticles. Based on the literature analysis, it was determined that T_{max} for SBR rubbers is approximately 449 °C [41] and, for EPDM rubbers, T_{max} = 409 °C [42]. In the conducted analyses in this article, it is not possible to unequivocally determine the qualitative composition of the rubber due to the diverse composition of the collected samples. The residual residue mainly consists of black carbon and other fillers. A multi-step curve profile is observed for the isopropanol extract, resulting from the extraction of a wide range of compounds. In the initial stage, the elimination of volatile substances such as organic solvents is observed. In the temperature range of 200–500 °C, the greatest mass loss, exceeding 55%, is observed, which is attributed to the overlapping thermal processes occurring in the tested samples. Degradation of polymers and medium-volatile materials such as elastomers and curing agents is observed within this temperature range [43]. Additives present in the tire composition, such as oils (including naphthenic oil, paraffinic oil, and highly aromatic oil), plasticizers, low molecular weight oligomers, emulsifiers, waxes, and antioxidants, undergo a process of evaporation due to the elevated temperature. Above the temperature of 550 °C, decomposition of remaining inorganic compounds (non-volatile materials, metal oxides, etc.) occurs. In the range of 720–820 °C (T_{max} = 769.6 °C), a peak is observed, likely originating from the decomposition of calcium carbonate to calcium oxide, indicating the presence of carbonate material [44]. In some cases, calcium carbonate is used as an additive in rubber mixtures. During thermal analysis in an oxidizing atmosphere for chloromethane extract, initially, desorption of volatile compounds is observed. Subsequently, similar to what occurred in an inert atmosphere, polymer degradation is observed. Additionally, in the air atmosphere, an additional peak was observed on the DTG curve at T_{max} = 538.8 °C originating from the combustion of carbon black, extracted solely using DCM [45]. It has been observed that in the case of extracts obtained using dichloromethane, a high content of carbon black is observed, whereas in the case of extracts obtained solely using isopropanol, lighter molecules present in the rubber composition, such as plasticizers, oils, etc., are washed away.

Figures 9 and 10 present thermogravimetric curves for the SZY, UMU, BIS, and CZT2 sediments. A multi-stage decomposition is observed, which is a result of the complex nature of the samples in terms of their varied compositions, types, and collection locations (Tables 6 and 7). The analysis of the SZY and UMU samples, collected as sand from areas near busy streets, shows similar degradation mechanisms (five-stage sample decomposition). The first stage of decomposition, in the temperature range of 30–150 °C, corresponds to the phase of dehydration and desorption of volatile substances. The next stage, occurring in the temperature range of 190–540 °C, is characterized by the presence of two peaks and is associated with the decomposition of organic matter, as well as remaining rubber particles that were not extracted due to their larger particle sizes. Samples with the largest grain fraction (250 μm–1 mm) show the highest percentage content of organic matter among the studied sediments. Above a temperature of 600 °C, the thermal decomposition of carbonates begins. The residual mass consists of inorganic residues, which occur in soils and car pollutants.
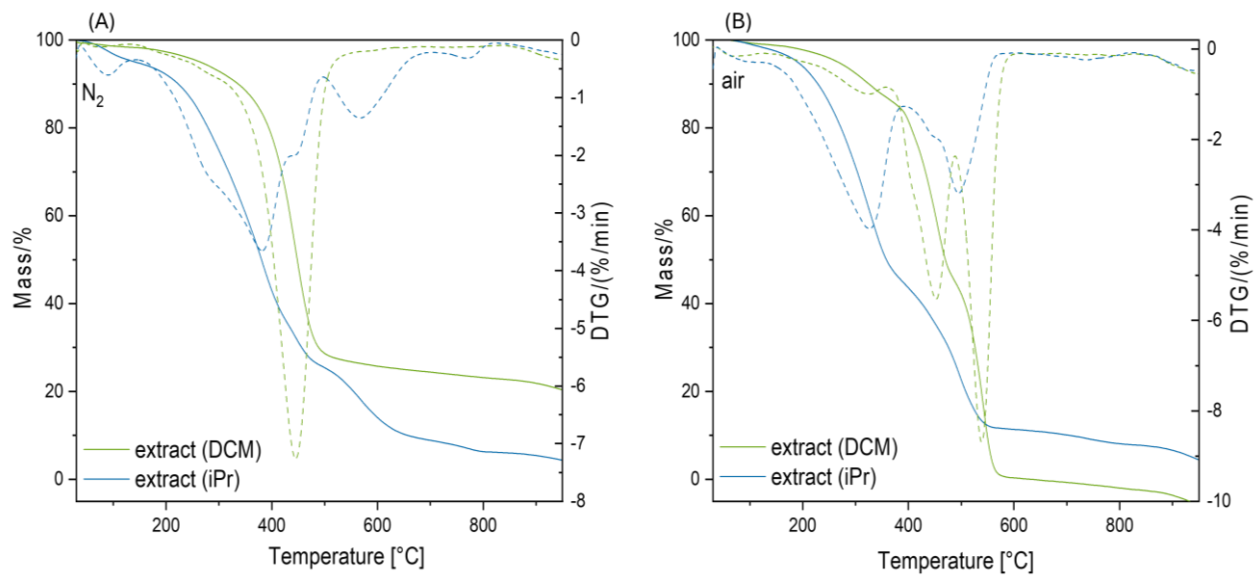
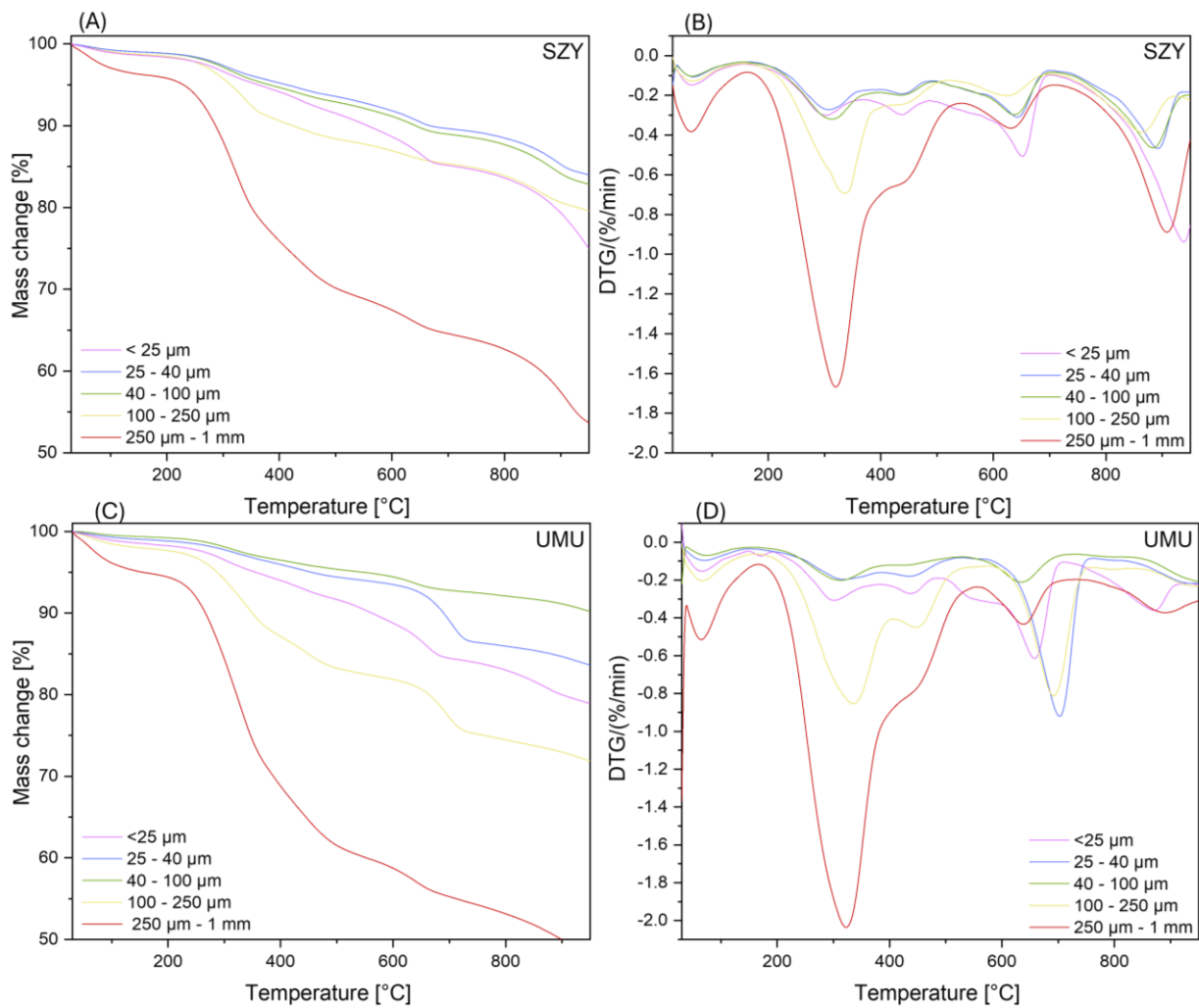**Figure 8.** TGA results of extracts (**A**) in a nitrogen atmosphere, (**B**) in an air atmosphere.

Figure 9. TGA results in a nitrogen atmosphere. For the SZY sample: (**A**) mass change, (**B**) DTG curve. For the UMU sample: (**C**) mass change, (**D**) DTG curve.
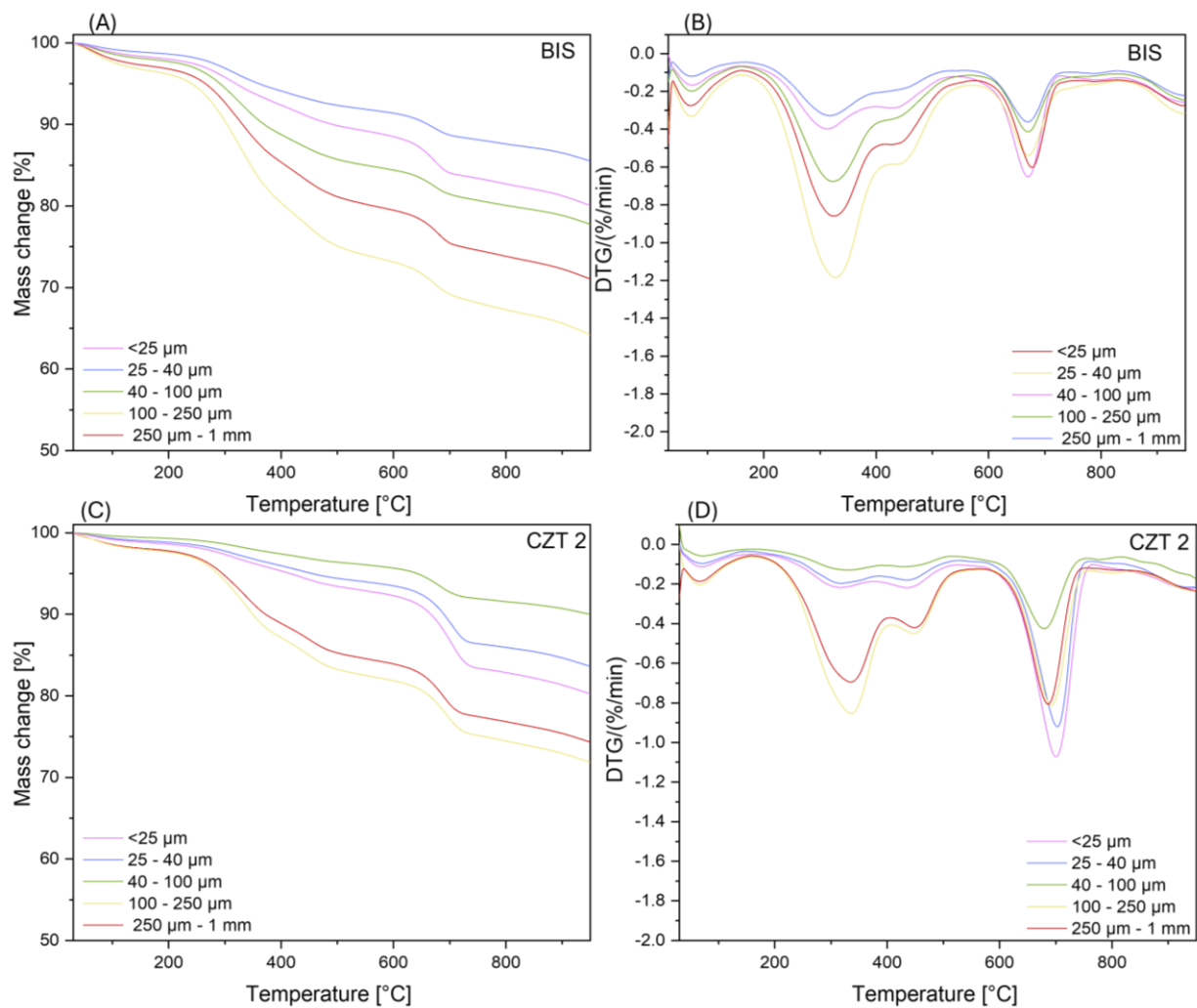
Figure 10. TGA results in a nitrogen atmosphere. For the BIS sample: (**A**) mass change, (**B**) DTG curve. For the CZT2 sample: (**C**) mass change, (**D**) DTG curve.

Table 6. TGA results data for the SZY and UMU samples.

SZY	T_{max1} [°C]	T_{max2} [°C]	T_{max3} [°C]	T_{max4} [°C]	T_{max5} [°C]
<25 μm	64.7	302.7	437.9	652.3	939.1
25–40 μm	65.3	308.6	438.4	642.2	893.1
40–100 μm	65.9	312.8	435.3	636.9	883.8
100–250 μm	63.6	335.7	438.4	624.3	866.4
250 μm–1 mm	62.5	319.9	440.2	630.1	908.7
UMU	T_{max1} [°C]	T_{max2} [°C]	T_{max3} [°C]	T_{max4} [°C]	T_{max5} [°C]
<25 μm	64.7	299.8	437.7	657.5	871.6
25–40 μm	67.9	308.5	432.3	646.5	925.3
40–100 μm	74.8	311.2	430.8	633.8	-
100–250 μm	70.1	316.9	431.9	641.9	858.2
250 μm–1 mm	65.2	322.7	442.2	639.1	

The BIS and CZT2 samples, collected, respectively, as sand and snow, differ slightly in the range of higher temperatures from samples collected as sand occurring near busy streets. The first stage of decomposition, in the temperature range of 30–150 °C, is analogous to the SZY and UMU samples and corresponds to the phase of dehydration and desorption of volatile substances. The second stage (190–540 °C) is associated with the decomposition of organic matter, as well as remaining rubber particles that were not extracted due to

their larger particle sizes. Above a temperature of 600 °C, one peak is observed, not two as in the case of UMU and SZY, which indicates a less diversified occurrence of inorganic compounds.

Table 7. TGA results data for the CZT2 and BIS samples.

CZT2	T_{max1} [°C]	T_{max2} [°C]	T_{max3} [°C]	T_{max4} [°C]
<25 μm	67.9	316.3	435.0	700.3
25–40 μm	69.8	319.1	438.2	703.2
40–100 μm	72.6	326.3	442.3	680.0
100–250 μm	66.5	336.0	448.0	691.3
250 μm–1 mm	66.2	335.9	449.4	686.4
BIS	T_{max1} [°C]	T_{max2} [°C]	T_{max3} [°C]	T_{max4} [°C]
<25 μm	71.9	310.6	428.6	670.6
25–40 μm	70.5	317.0	433.0	668.4
40–100 μm	71.5	323.0	437.0	669.5
100–250 μm	70.6	327.3	431.7	669.7
250 μm–1 mm	69.3	324.4	433.7	678.0

3.4. Spectroscopic Analysis

3.4.1. NMR Spectroscopy

^{1}H NMR spectroscopy was employed to determine the qualitative composition of a mixture of substances contained in extracts obtained after washing with dichloromethane (DCM) and isopropanol (iPrOH) (Figure 11). The spectra showed significant similarities, but with differences in their intensity. All the spectra obtained exhibited intense signals from aliphatic chains in the range of 0–3 ppm.
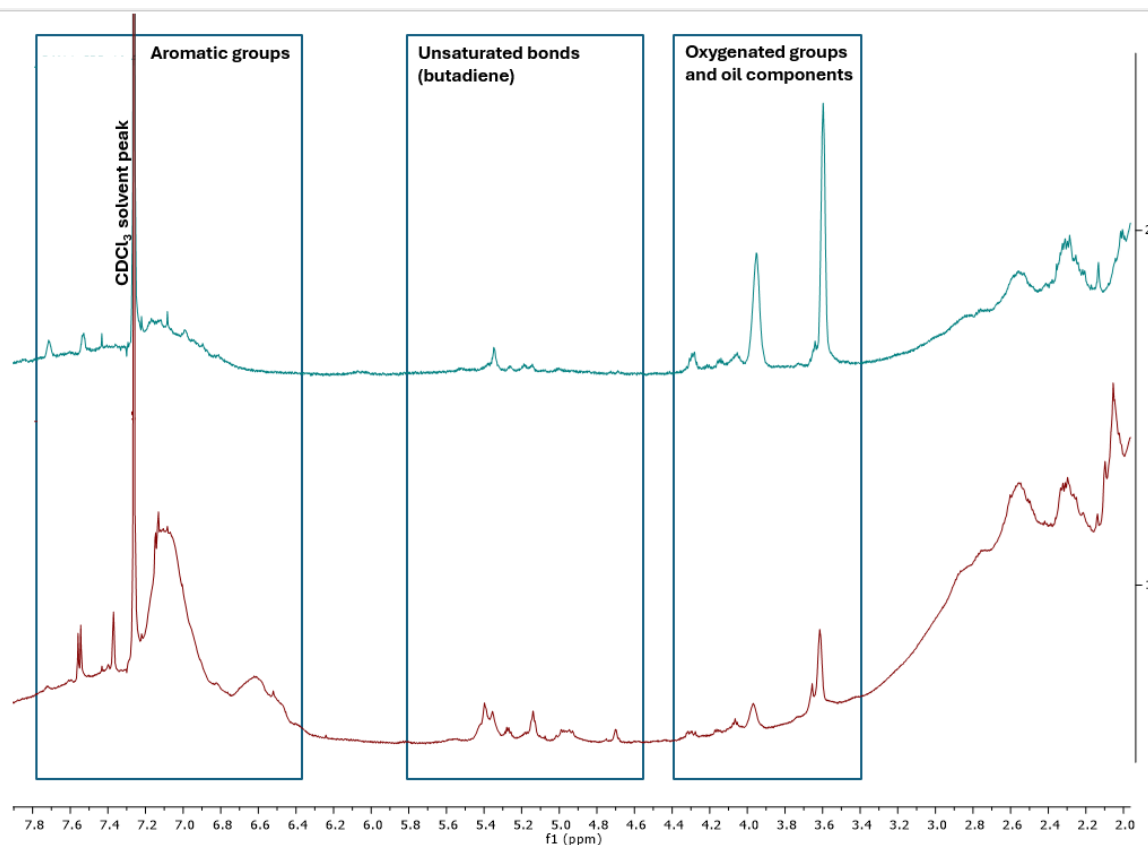

Figure 11. NMR spectroscopy of extracts obtained from fractions extracted with DCM (red) and iPrOH (blue).

Furthermore, the region from 3 to 8 ppm can be divided into distinct signal groups: (a) 3.4–4.4 ppm from oxygenated groups and oil components; (b) 4.6–5.6 ppm from butadiene derivatives; (c) 6.4–7.8 ppm from aromatic groups.

The qualitative composition indicates the presence of organic residues that contain substances that are part of the composition of tires. The data presented here are consistent with those available in the literature, suggesting a commonality in the composition of such extracts [23].

3.4.2. FT-IR Spectroscopy

The FT-IR spectra of TRWP obtained through iPr and DCM extraction are presented in Figure 12. Similar to the observations made by NMR spectroscopy, no significant differences in the qualitative composition of both samples are discernible. The spectra exhibit signals from aliphatic hydrocarbons at 2921 cm^{-1}, 2852 cm^{-1} (C-H stretching), and 1456 cm^{-1} (C-H bending). Above 3000 cm^{-1}, a weakly intense band from aromatic bonds can be observed. Unsaturated bonds (C=C) also appear in the band below 1600 cm^{-1}. The band around 1700 cm^{-1} corresponds to carbonyl groups. These signals align with the anticipated content, primarily composed of residues of micro- and nanoparticles generated due to tire wear (i.e., polymers, such as the previously discussed butadiene, and process oils) [46].
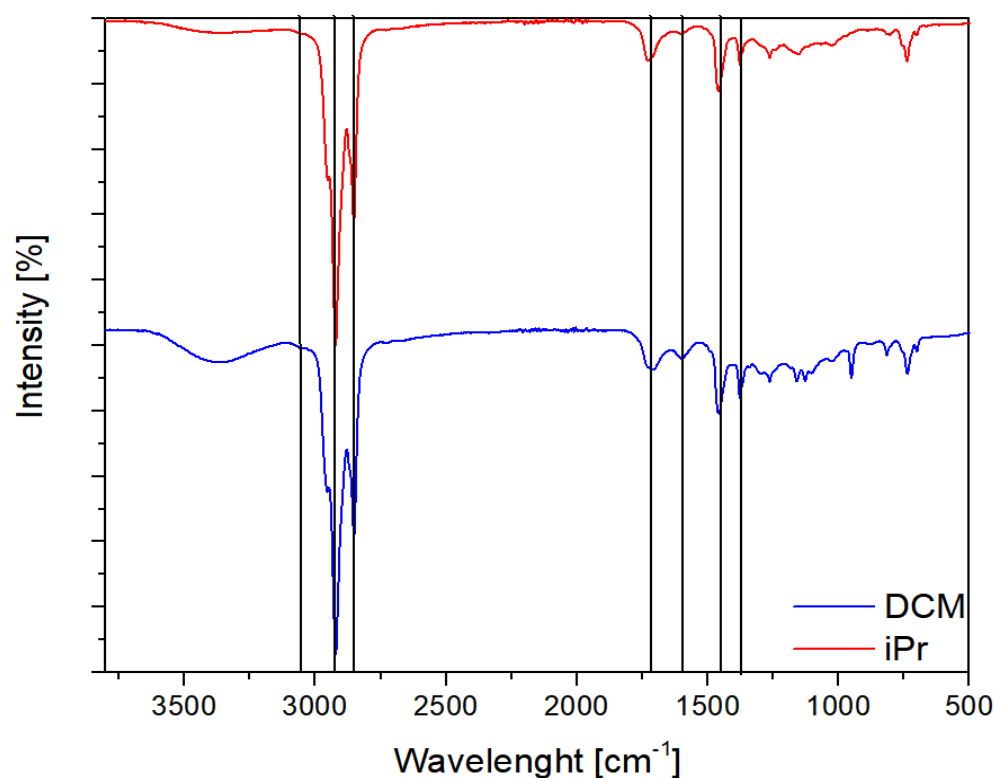

Figure 12. FT-IR spectroscopy of extracts obtained from fractions extracted with DCM and iPrOH.

3.4.3. XRD Analysis

Figure 13 shows the XRD analysis of the selected samples. The XRD results of the UMU and CZT2 samples are similar. There are peaks from the same phases: Si_2O, Fe_2O_3, and $CaSi_2O_6$. They differ only in the intensity of the peaks. In the sample SZY, in addition to peaks from Si_2O, $CaSi_2O_6$, and Fe_2O_3, there is also a reflection from SiC. Similar results were presented in the work of Guleria et al. [47], which analyzed tire chips with other additives. The XRD analysis presented in the work of Guleria et al. shows that the tires contain the same compounds as in the results presented in this paper. Moreover, in the work of Amir et al. [48] XRD of rubber from recycled tires was also examined. In the results

of Amir et al. the occurrence of $CaCO_3$ and $CaSi_2O_6$ compounds in the tested tires was shown; these compounds also appear in the XRD reflections in this work.
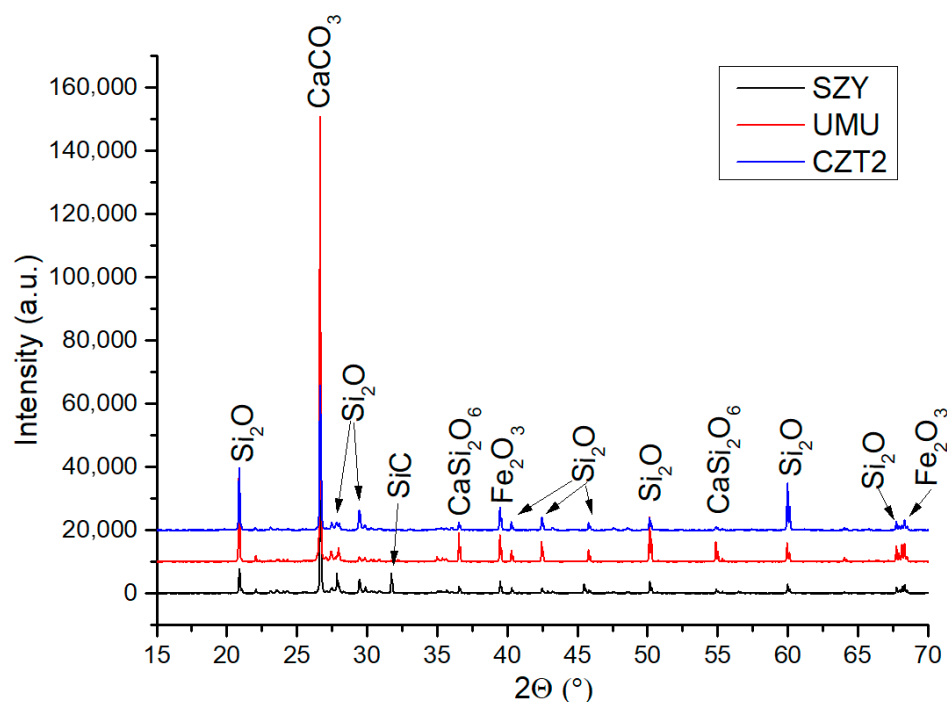

Figure 13. X-ray diffraction of the analyzed samples.

4. Conclusions

This research paper provides a comprehensive investigation into the characteristics of micro- and nano-pollutants, focusing on those originating from the degradation of tires and roads in winter season. The study was conducted in Poznań, Poland, characterized by transitional and temperate climatic conditions.

During this period, the streets are typically treated with salt to mitigate ice formation, and the majority of private vehicle users transition to softer tires. These factors contribute to an accelerated rate of tire degradation, leading to an increased generation of the pollutants under investigation.

The initial phase of the study involved the extraction of micro- and nano-pollutants from collected sediments, including snow, sand, and standing water, using organic solvents. The resulting solutions were then analyzed to determine their concentration, particle size, and qualitative composition, utilizing spectroscopic techniques for a comprehensive characterization. The residue, primarily composed of sand and residual organic matter, was left after the extraction process. This residue underwent extensive analysis to identify its composition.

The pollutants characterized in this study exhibited a diverse chemical composition and a broad size range, spanning from 1mm to as small as 1 nm. EDS mapping revealed that the primary fraction consisted of sand and organic compounds. Traces of iron were also detected, likely originating from the wear of brake pads and discs. Spectroscopic studies of the extracted particles confirmed the presence of tire rubber residues. DLS studies showed that a smaller particle size characterizes the extracts obtained during DCM washing. The EDS identified only carbon in these samples. Thermogravimetric analysis of the extracts allowed for the determination that the DCM fraction contains a high concentration of carbon black, while lighter particles such as oils and plasticizers transition to the iPr-OH fraction.

An intriguing observation made during the study was the role of snow in the collection of these pollutants. It was noted that the presence of snow near roads appeared to inhibit

the migration of pollutants, thereby acting as a filter and capturing/agglomerating a larger quantity of particles.

A particularly surprising finding of the study was the primary source of the pollutants found in the accumulated snow sediment, as depicted in Figure 14. Contrary to initial expectations, the majority of these pollutants were traced back to worn tires and asphalt, rather than from exhaust gases and oils produced during driving. This finding underscores the significant environmental impact of tire and road wear, highlighting an area that warrants further investigation and action.

Figure 14. Snow deposits accumulate while driving on road vehicles.

In conclusion, this study provides valuable insights into the nature and sources of micro- and nano-pollutants and underscores the need for more sustainable practices in road maintenance and vehicle usage. It is anticipated that these findings will stimulate further research in this field and inform decisions aimed at mitigating environmental pollution.

References

1. Baensch-Baltruschat, B.; Kocher, B.; Stock, F.; Reifferscheid, G. Tyre and Road Wear Particles (TRWP)—A Review of Generation, Properties, Emissions, Human Health Risk, Ecotoxicity, and Fate in the Environment. *Sci. Total Environ.* **2020**, *733*, 137823. [CrossRef] [PubMed]
2. Milani, M.; Pucillo, F.P.; Ballerini, M.; Camatini, M.; Gualtieri, M.; Di Martino, S.F. First Evidence of Tyre Debris Characterization at the Nanoscale by Focused Ion Beam. *Mater. Charact.* **2004**, *52*, 283–288. [CrossRef]
3. Sarkissian, G. The Analysis of Tire Rubber Traces Collected After Braking Incidents Using Pyrolysis-Gas Chromatography/Mass Spectrometry. *J. Forensic Sci.* **2007**, *52*, 1050–1056. [CrossRef]
4. De Oliveira, T.; Muresan, B.; Ricordel, S.; Lumière, L.; Truong, X.-T.; Poirier, L.; Gaspéri, J. Realistic Assessment of Tire and Road Wear Particle Emissions and Their Influencing Factors on Different Types of Roads. *J. Hazard. Mater.* **2024**, *465*, 133301. [CrossRef] [PubMed]
5. Stalnaker, D.O.; Turner, J.L.; Parekh, D.; Whittle, B.; Norton, R. Indoor Simulation of Tire Wear: Some Case Studies. *Tire Sci. Technol.* **1996**, *24*, 94–118. [CrossRef]
6. Wik, A.; Dave, G. Occurrence and Effects of Tire Wear Particles in the Environment—A Critical Review and an Initial Risk Assessment. *Environ. Pollut.* **2009**, *157*, 1–11. [CrossRef] [PubMed]
7. Panko, J.M.; Chu, J.; Kreider, M.L.; Unice, K.M. Measurement of Airborne Concentrations of Tire and Road Wear Particles in Urban and Rural Areas of France, Japan, and the United States. *Atmos. Environ.* **2013**, *72*, 192–199. [CrossRef]
8. Wagner, S.; Hüffer, T.; Klöckner, P.; Wehrhahn, M.; Hofmann, T.; Reemtsma, T. Tire Wear Particles in the Aquatic Environment—A Review on Generation, Analysis, Occurrence, Fate and Effects. *Water Res.* **2018**, *139*, 83–100. [CrossRef]
9. Hays, M.D.; Cho, S.-H.; Baldauf, R.; Schauer, J.J.; Shafer, M.M. Particle Size Distributions of Metal and Non-Metal Elements in an Urban Near-Highway Environment. *Atmos. Environ.* **2011**, *45*, 925–934. [CrossRef]
10. Wi, E.; Park, E.; Shin, H.; Hong, J.; Jeong, S.; Kwon, J.-T.; Lee, H.-J.; Lee, J.; Kim, Y. Overall Distribution of Tire-Wear Particles, Nanocarbon Black, and Heavy Metals in Size-Fractionated Road Dust Collected from Steel Industrial Complexes. *Sci. Total Environ.* **2023**, *884*, 163878. [CrossRef]
11. Harrison, R.M.; Jones, A.M.; Gietl, J.K.; Yin, J.; Green, D.C. Estimation of the Contributions of Brake Dust, Tire Wear, and Resuspension to Nonexhaust Traffic Particles Derived from Atmospheric Measurements. *Environ. Sci. Technol.* **2012**, *46*, 6523–6529. [CrossRef] [PubMed]
12. Councell, T.B.; Duckenfield, K.U.; Landa, E.R.; Callender, E. Tire-Wear Particles as a Source of Zinc to the Environment. *Environ. Sci. Technol.* **2004**, *38*, 4206–4214. [CrossRef] [PubMed]
13. Adachi, K.; Tainosho, Y. Characterization of Heavy Metal Particles Embedded in Tire Dust. *Environ. Int.* **2004**, *30*, 1009–1017. [CrossRef] [PubMed]
14. ADAC. Tyre Wear Particles in the Environment. 2022. Available online: https://assets.adac.de/image/upload/v1639663105/ADAC-eV/KOR/Text/PDF/Tyre_wear_particles_in_the_environment_zkmd3a.pdf (accessed on 8 April 2024).
15. Dumont, E.R.; Gao, X.; Zheng, J.; Macairan, J.; Hernandez, L.M.; Baesu, A.; Bayen, S.; Robinson, S.A.; Ghoshal, S.; Tufenkji, N. Unraveling the Toxicity of Tire Wear Contamination in Three Freshwater Species: From Chemical Mixture to Nanoparticles. *J. Hazard. Mater.* **2023**, *453*, 131402. [CrossRef] [PubMed]
16. Knight, L.J.; Parker-Jurd, F.N.F.; Al-Sid-Cheikh, M.; Thompson, R.C. Tyre Wear Particles: An Abundant yet Widely Unreported Microplastic? *Environ. Sci. Pollut. Res. Int.* **2020**, *27*, 18345–18354. [CrossRef] [PubMed]
17. Järlskog, I.; Jaramillo-Vogel, D.; Rausch, J.; Gustafsson, M.; Strömvall, A.-M.H.; Andersson-Sköld, Y. Concentrations of Tire Wear Microplastics and Other Traffic-Derived Non-Exhaust Particles in the Road Environment. *Environ. Int.* **2022**, *170*, 107618. [CrossRef] [PubMed]
18. Bouredji, A.; Pourchez, J.; Forest, V. Biological Effects of Tire and Road Wear Particles (TRWP) Assessed by in Vitro and in Vivo Studies—A Systematic Review. *Sci. Total Environ.* **2023**, *894*, 164989. [CrossRef]
19. Liu, Y.; Chen, H.; Gao, J.; Liu, Y.; Dave, K.; Chen, J.; Federici, M.; Perricone, G. Comparative Analysis of Non-Exhaust Airborne Particles from Electric and Internal Combustion Engine Vehicles. *J. Hazard. Mater.* **2021**, *420*, 126626. [CrossRef]
20. Obereigner, G.; Shorten, R.; Meier, F.; Jones, S.; Wikström, N.; Del Re, L. *Active Limitation of Tire Wear and Emissions for Electrified Vehicles*; SAE Technical Paper Serie; SAE International: Warrendale, PA, USA, 2021. [CrossRef]
21. Rødland, E.S.; Lind, O.C.; Reid, M.J.; Heier, L.S.; Okoffo, E.D.; Rauert, C.; Thomas, K.V.; Meland, S. Occurrence of Tire and Road Wear Particles in Urban and Peri-Urban Snowbanks, and Their Potential Environmental Implications. *Sci. Total Environ.* **2022**, *824*, 153785. [CrossRef]
22. Vijayan, A.; Österlund, H.; Magnusson, K.; Maršálek, J.; Viklander, M. Microplastics (MPs) in Urban Roadside Snowbanks: Quantities, Size Fractions and Dynamics of Release. *Sci. Total Environ.* **2022**, *851*, 158306. [CrossRef]
23. Calarnou, L.; Traïkia, M.; Leremboure, M.; Malosse, L.; Dronet, S.; Delort, A.-M.; Besse-Hoggan, P.; Eyheraguibel, B. Assessing Biodegradation of Roadway Particles via Complementary Mass Spectrometry and NMR Analyses. *Sci. Total Environ.* **2023**, *900*, 165698. [CrossRef]
24. Thomas, J.; Moosavian, S.K.; Cutright, T.J.; Pugh, C.; Soucek, M.D. Method Development for Separation and Analysis of Tire and Road Wear Particles from Roadside Soil Samples. *Environ. Sci. Technol.* **2022**, *56*, 11910–11921. [CrossRef] [PubMed]

25. Rødland, E.S.; Lind, O.C.; Reid, M.J.; Heier, L.S.; Skogsberg, E.; Snilsberg, B.; Gryteselv, D.; Meland, S. Characterization of Tire and Road Wear Microplastic Particle Contamination in a Road Tunnel: From Surface to Release. *J. Hazard. Mater.* **2022**, *435*, 129032. [CrossRef]

26. Kim, G.; Lee, S.-H. Characteristics of Tire Wear Particles Generated by a Tire Simulator under Various Driving Conditions. *Environ. Sci. Technol.* **2018**, *52*, 12153–12161. [CrossRef] [PubMed]

27. Park, I.-Y.; Kim, H.; Lee, S.-H. Characteristics of Tire Wear Particles Generated in a Laboratory Simulation of Tire/Road Contact Conditions. *J. Aerosol Sci.* **2018**, *124*, 30–40. [CrossRef]

28. Tonegawa, Y.; Sasaki, S. Development of Tire-Wear Particle Emission Measurements for Passenger Vehicles. *Emiss. Control Sci. Technol.* **2021**, *7*, 56–62. [CrossRef]

29. Klöckner, P.; Seiwert, B.; Eisentraut, P.; Braun, U.; Reemtsma, T.; Wagner, S. Characterization of Tire and Road Wear Particles from Road Runoff Indicates Highly Dynamic Particle Properties. *Water Res.* **2020**, *185*, 116262. [CrossRef]

30. Mennekes, D.; Nowack, B. Tire Wear Particle Emissions: Measurement Data Where Are You? *Sci. Total Environ.* **2022**, *830*, 154655. [CrossRef]

31. Marwood, C.A.; McAtee, B.L.; Kreider, M.L.; Ogle, R.S.; Finley, B.L.; Sweet, L.; Panko, J.M. Acute Aquatic Toxicity of Tire and Road Wear Particles to Alga, Daphnid, and Fish. *Ecotoxicol.* **2011**, *20*, 2079–2089. [CrossRef]

32. Yang, K.; Jing, S.; Liu, Y.; Yan, M.; Yi, X.; Liu, L. Acute Toxicity of Tire Wear Particles, Leachates and Toxicity Identification Evaluation of Leachates to the Marine Copepod, *Tigriopus japonicus*. *Chemosphere* **2022**, *297*, 134099. [CrossRef]

33. Halle, L.L.; Palmqvist, A.; Kampmann, K.; Jensen, A.A.; Hansen, T.; Khan, F.R. Tire Wear Particle and Leachate Exposures from a Pristine and Road-Worn Tire to Hyalella Azteca: Comparison of Chemical Content and Biological Effects. *Aquat. Toxicol.* **2021**, *232*, 105769. [CrossRef] [PubMed]

34. Panko, J.M.; Kreider, M.L.; McAtee, B.L.; Marwood, C.A. Chronic Toxicity of Tire and Road Wear Particles to Water- and Sediment-Dwelling Organisms. *Ecotoxicology* **2012**, *22*, 13–21. [CrossRef]

35. Cunningham, B.; Harper, B.; Brander, S.M.; Harper, S.L. Toxicity of Micro and Nano Tire Particles and Leachate for Model Freshwater Organisms. *J. Hazard. Mater.* **2022**, *429*, 128319. [CrossRef] [PubMed]

36. Day, K.E.; Holtze, K.E.; Metcalfe-Smith, J.L.; Bishop, C.; Dutka, B.J. Toxicity of Leachate from Automobile Tires to Aquatic Biota. *Chemosphere* **1993**, *27*, 665–675. [CrossRef]

37. Khan, F.R.; Halle, L.L.; Palmqvist, A. Acute and Long-Term Toxicity of Micronized Car Tire Wear Particles to *Hyalella azteca*. *Aquat. Toxicol.* **2019**, *213*, 105216. [CrossRef]

38. Gualtieri, M.; Andrioletti, M.; Vismara, C.; Milani, M.; Camatini, M. Toxicity of Tire Debris Leachates. *Environ. Int.* **2005**, *31*, 723–730. [CrossRef]

39. Mian, H.R.; Chippi-Shreshta, G.; McCarty, K.; Hewage, K.; Sadiq, R. An Estimation of Tire and Road Wear Particles Emissions in Surface Water Based on a Conceptual Framework. *Sci. Total Environ.* **2022**, *848*, 157760. [CrossRef]

40. Filella, M.; Reimann, C.; Biver, M.; Rodushkin, I.; Rodushkina, K. Tellurium in the Environment: Current Knowledge and Identification of Gaps. *Environ. Chem.* **2019**, *16*, 215. [CrossRef]

41. Yin, B.; Wang, J.; Jia, H.; He, J.; Zhang, X.; Xu, Z. Enhanced Mechanical Properties and Thermal Conductivity of Styrene–Butadiene Rubber Reinforced with Polyvinylpyrrolidone-Modified Graphene Oxide. *J. Mater. Sci.* **2016**, *51*, 5724–5737. [CrossRef]

42. Yan, C.; Chen, B.; Li, X.; He, J.; Zhao, X.; Zhu, Y.; Yang, R. Silicon Hybrid EPDM Composite with High Thermal Protection Performance. *Polymers* **2024**, *16*, 695. [CrossRef]

43. Mis-Fernández, R.; Azamar-Barrios, J.A.; Ríos-Soberanis, C.R. Characterization of the Powder Obtained from Wasted Tires Reduced by Pyrolysis and Thermal Shock Process. *J. Appl. Res. Technol.* **2008**, *6*, 95–104. [CrossRef]

44. Characterization of EPDM Rubber by TGA and Hi-Res' TGA. Available online: https://www.tainstruments.com/pdf/literature/TS-79.pdf (accessed on 8 April 2024).

45. Cataldo, F. On the Characterisation of Carbon Black from Tire Pyrolysis. *Fuller. Nanotub. Carbon Nanostruct./Fuller. Nanotub. Carbon Nanostruct.* **2019**, *28*, 368–376. [CrossRef]

46. Kyari, M.Z.; Cunliffe, A.A.; Williams, P.T. Characterization of Oils, Gases, and Char in Relation to the Pyrolysis of Different Brands of Scrap Automotive Tires. *Energy Fuels* **2005**, *19*, 1165–1173. [CrossRef]

47. Guleria, S.P.; Dutta, R.K. Unconfined Compressive Strength of Fly Ash–Lime–Gypsum Composite Mixed with Treated Tire Chips. *J. Mater. Civ. Eng.* **2011**, *23*, 1255–1263. [CrossRef]

48. Amir, A.; Saad, N.H.; Ramli, A.S.; Abd Rashid, A.; Yusoff, N.; Abdullah, N.R.; Kasolang, S.; Jaffar, A. Thermal and rheological behavior of recycled rubber/natural rubber blends in recycle tire process. *J. Teknol.* **2015**, *76*, 89–94. [CrossRef]